Journal of Alloys and Compounds 509 (2011) 2232–2237

Contents lists available at ScienceDirect

Journal of Alloys and Compounds

journal homepage: www.elsevier.com/locate/jallcom

Synthesis, characterization, and microwave dielectric properties of $Mg_4Nb_2O_9$ ceramics produced through the aqueous sol–gel process

H.T. Wu[a,b], L.X. Li[a,*], Q. Zou[a], Q.W. Liao[a], P.F. Ning[a], P. Zhang[a]

[a] School of Electric and Information Engineering, Tianjin University, Tianjin 300072, China
[b] School of Materials Science and Engineering, University of Jinan, Jinan 250022, China

ARTICLE INFO

Article history:
Received 20 July 2010
Received in revised form 28 October 2010
Accepted 29 October 2010
Available online 10 November 2010

Keywords:
Magnesium niobate
Nanopowder synthesis
Sol–gel process
Microwave dielectric properties

ABSTRACT

Microwave dielectric ceramics of $Mg_4Nb_2O_9$ were prepared by the sol–gel method and their microwave dielectric properties and microstructure were investigated in this study. Firstly, highly reactive nano-sized magnesium niobate powders were successfully synthesized at 550 °C in oxygen atmosphere with particle size of 30–40 nm. And the phase formation was investigated by means of DTA–TG and XRD analyses. Subsequently, the sintering ability and microwave dielectric properties of $Mg_4Nb_2O_9$ ceramics were studied under various sintering temperatures ranging from 1150 °C to 1325 °C. As the sintering temperature increased from 1150 °C to 1325 °C, the density values, the ε_r values and the *Qf* values increased and saturated at 1250 °C, whereas the *Qf* values decreased at the sintering temperature above 1300 °C .The τ_f values were ranged from −48.7 to −37.8 ppm/°C. Due to the increased density and appropriate grain growth the $Mg_4Nb_2O_9$ ceramics sintered at 1250 °C had the excellent microwave dielectric properties of ε_r = 12.3, *Qf* = 165,000 GHz and τ_f = −47.5 ppm/°C. The results showed that the sintering temperature was significantly reduced by the sol–gel process.

1. Introduction

The rapid progress in mobile and satellite communication system has been creating a high demand for the development of microwave dielectric materials with a high quality factor, an appropriate dielectric constant, and a near-zero temperature coefficient of resonant frequency. The corundum-like phase of magnesium niobate ($Mg_4Nb_2O_9$; MN) with a high *Qf*, is a suitable material for microwave applications, such as substrates and resonators at high frequency, because the dielectric constant and quality factor values are comparable to those of sintered Al_2O_3 [1]. The present research about MN phase synthesized by the conventional solid-state method were reported elsewhere [2–4] and the MN ceramic was investigated to possess a ε_r of ∼12.4, a τ_f of ∼−70 ppm/°C and in particular, a high *Qf* of ∼193,000 GHz [5]. However, it also required a sintering temperature of as high as 1350–1400 °C/10 h. Similarly, Khalam et al. [6] reported that the MN ceramic was sintered at 1400 °C with a *Qf* result of 116,000 GHz. Obviously the high sintering temperature of the ceramics will limit its applications for practical cases and the reduction of the sintering temperature is desirable to enable commercial applications such as in integrated circuits. Usually it is believed that lowering the sintering temperature can be achieved by chemical processing, adding glass flux, and using starting materials with smaller particle sizes. As we known, adding glass flux usually causes the detrimental effect on the microwave properties of ceramics. So much attention has been paid to chemical processing and other special milling method [7,8] using starting materials with smaller particle sizes.

And now there have been many investigations of the chemical processing methods [9–13], which have been developed as alternatives to the conventional solid state reaction of mixed oxides for producing ceramics to reduce the sintering temperature. For example, the MN ceramic was successfully fabricated at 950 °C for 2 h in air by the precipitation process with ε_r = 8.5, *Qf* = 5500 GHz [9] and by a hydrothermal method the MN ceramic was obtained with the highest *Qf* value of 26,069 GHz at 1300 °C [12]. Among the methods of wet chemical techniques, the sol–gel is undoubtedly one of a useful process for producing powders with a good control over stoichiometry and homogeneity, yielding nano-sized particles. For example, Wu et al. [14] recently reported that nano-sized B_2O_3-doped $ZnTiO_3$ particles were successfully synthesized through the sol–gel technique at 800 °C and Zhang et al. [15] reported that a sol–gel process was adopted to synthesize nanopowders with composition of $(1-x)(Ca_{0.61},Nd_{0.26})TiO_3 - x(Nd_{0.55},Li_{0.35})TiO_3$. Dense ceramics synthesized by the nanoparticles could be achieved at low-temperature of 1150 °C due to the effect of small size nanoparticles. Similarly, the sol–gel process was widely used in many other ceramic systems [16–19]. However, few researches about the microwave properties of the MN ceramic fabricated by the

* Corresponding author. Tel.: +86 22 2740 2838; fax: +86 22 2740 1233.
E-mail address: mse_wuht@ujn.edu.cn (L.X. Li).

0925-8388/$ – see front matter © 2010 Elsevier B.V. All rights reserved.
doi:10.1016/j.jallcom.2010.10.191

sol–gel process were reported in the present literature. The goal of this research was to explore the capabilities of sol–gel method, for reducing the sintering temperature. The influence of sintering temperature on the crystalline phase, microstructure, and microwave dielectric properties of MN ceramics was investigated. The results showed that the aqueous sol–gel process was the most effective and least expensive technique used for the preparation of MN ceramics with low sintering temperature.

2. Experimental

Samples with composition of MN ceramics were prepared through the sol–gel process, with high-purity (99.9%) $Mg(NO_3)_2{\cdot}6H_2O$ and Nb_2O_5 as raw materials. Firstly, Nb_2O_5 were weighed accurately according to the mass ratio and dissolved in the appropriate amount of HF after heating at hot water bath for 20 h and then the ammonia water was added into the above solutions in order to form chemical precipitate of niobic acid ($Nb(OH)_5$). Subsequently, the $Nb(OH)_5$ precipitate was filtered off and washed with distilled water for six times to remove the H^+ and F^+ ions and then dissolved completely in citric acid water solution by continuous magnetic stirring at 300 rpm for 15 min. Meanwhile, a stoichiometric amount of $Mg(NO_3){\cdot}6H_2O$ was added to the above solution and then the solution was stirred for another 30 min. Finally, the ethyl alcohol (20–40 ml) was added to the as-prepared mixed solution in drops and stirred for 1 h to form a transparent and stable sol. pH of the solution was maintained in the range of 3.5–5 by adding buffering agents. The sol was heated at 80–90 °C for about 1 h to obtain a xerogel. The xerogel was decomposed at various temperatures ranging from 550 °C to 850 °C in a muffle furnace for crystallization. The as-prepared powers were ball milled in a polyethylene jar for 4 h using ZrO_2 balls in ethanol medium to reduce the conglobation phenomena. The powders were then mixed with polyvinyl alcohol as a binder, granulated and pressed into cylindrical disks of 10 mm diameter and about 5 mm height at a pressure of about 200 MPa. These pellets were preheated at 600 °C for 4 h to expel the binder and then sintered at selected temperatures for 4 h in air at a heating rate of 5 °C/min.

In order to analyze the phase formation of MN ceramics, the as-formed MN xerogel was characterized using thermogravimetry (TG) and differential thermal analysis (DTA) to study its thermal properties. Phase analysis of the MN powder and ceramic was conducted with the help of a Rigaku diffractometer (Model D/Max-B, Rigaku Co., Japan) using Ni filtered Cu Kα radiation (λ = 0.1542 nm) at 40 kV and 40 mA settings. Based on the XRD analysis, the raw MN powder was examined for its morphology and particle size using a field emission scanning electron microscopy (Model Jeol JSM-7600F, FEI Co., Japan). The bulk densities of the sintered ceramics were measured by the Archimedes method. An HP8720ES network analyzer (Hewlett-Packard, Santa Rosa, CA) was used for the measurement of microwave dielectric properties. The dielectric constants were measured using the Hakki–Coleman post-resonator method by exciting the TE011 resonant mode of the dielectric resonator using the electric probe of an antenna as suggested by Hakki and Coleman and Courtney [20]. The unloaded quality factors were measured using the TE01d mode in the cavity method [21]. All the measurements were made at room temperature and in the frequency range 9–10 GHz. The temperature coefficients of the resonant frequency were measured at the temperature range of 25–85 °C.

3. Results and discussion

3.1. Phase formation and characterization of MN powders

Fig. 1 showed the TG–DTA curves of the MN xerogel in pure oxygen atmosphere at a heating rate of 10 °C/min. The results indicated that the obvious weight losses began at 80 °C and all chemical reactions involving weight losses, such as decomposition of the organic polymeric network with evolution of CO_2 and H_2O, were completed below 531.6 °C. The total weight loss was about 80%, which occurred in three steps: (i) initial weight loss (about 10%) below 250 °C, resulting from the evaporation of residual solvent and water, with wide and weak endothermic peaks from about 100 °C, (ii) a second significant weight loss (about 60% caused by the decomposition of the organic polymeric network with evolution of CO_2 and H_2O, with endothermic peaks ranging from 250 °C to 400 °C, and (iii) a third weight loss (about 10–20%) in the TG curves, combined with an exothermal peak at the temperature region of 400–531.6 °C, which was attributed to the oxidation of metal–organic groups. The similar TG results of MN xerogel were also reported in other microwave dielectric ceramics with citrate sol–gel method [14–17]. No further significant weight loss and thermometric peaks were observed above 531.6 °C in the TG–DTA

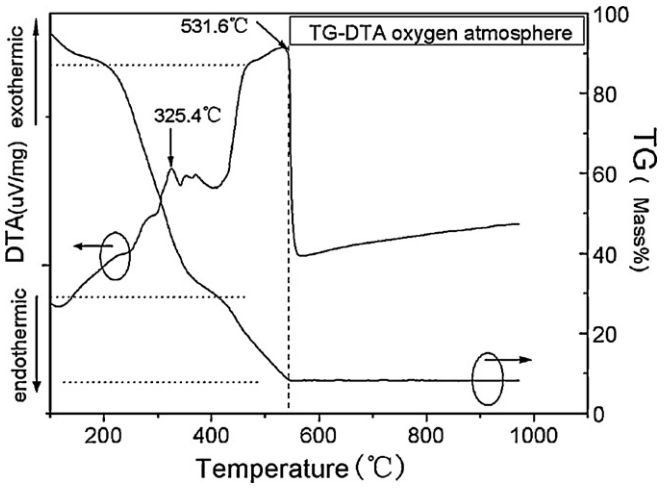

Fig. 1. TG–DTA curves of the MN gel in oxygen atmosphere.

curves, indicating the minimum firing temperature to synthesize the magnesium niobate phases. By comparison, the DTA results mentioned by other solid-state methods [2,3] meant different MN formation temperatures, all of which were above 600 °C.

Fig. 2 showed the XRD patterns of MN xerogel calcined in oxygen atmosphere ranging from 550 °C to 850 °C for 30 min. At 550 °C the crystallization of MN took place and this phenomenon was recognized from the exothermic peak of DTA and the corresponding TG profile as described above. The gel fired at 550 °C consisted of the predominant phases of $Mg_4Nb_2O_9$, which were matched with JCPDS file number 38-1459. A minor phase of $Mg_5Nb_4O_{15}$ with orthorhombic symmetry was developed accompanying $Mg_4Nb_2O_9$ as separated phases just at 30.16° and 31.30°.As the temperature increasing to 850 °C, the intensity of the $Mg_4Nb_2O_9$ peaks was gradually enhanced and the $Mg_5Nb_4O_{15}$ phase had been found to nearly disappear. Using the sol–gel method, we found that the calcination temperature was remarkably decreased to 550 °C, in comparison to these of the conventional mixed oxide route reported earlier [2–4,7,8] and other chemical methods [9–13] as shown in Table 1.

In Fig. 2 the influence of calcination temperature on X-ray diffraction of the samples was observed in the variations of intensity and full width at half maximum (FWHM) of the diffraction peaks. With increasing the firing temperature, the characteristic

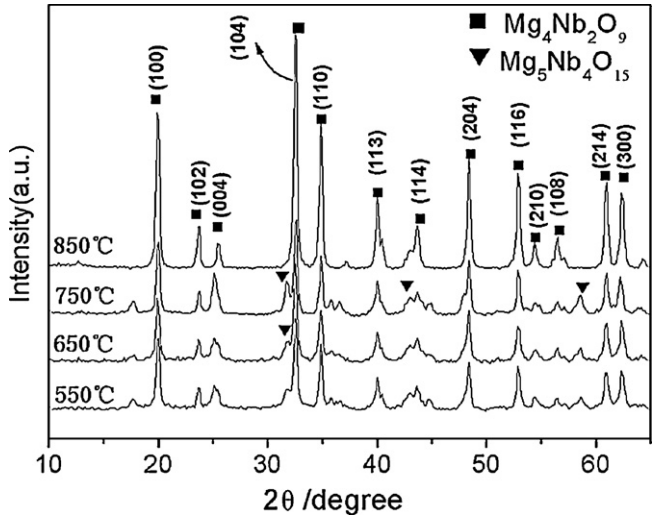

Fig. 2. X-ray diffraction patterns of the MN gel calcined at 550 °C, 650 °C, 750 °C, 850 °C for 30 min.

Table 1
Comparison of $Mg_4Nb_2O_9$ powders synthesized by different methods.

Method	Calcination temperature (°C)	Grain size (nm)	Refs.
Solid-state	900/1100/1300	–/300–730/–/	[2–4]
Vibro-milling	950	250–1000	[7]
Ball-milling	900	72.5	[8]
Precipitation	700/600	–/40	[9,10]
Coprecipitation	750	150	[11]
Hydrothermal synthesis	700	<100	[12]
Citrate gel	750	40	[13]
Sol–gel	550	35	Our results

"–" denoted that no values of grain size were mentioned.

peaks of (1 0 0) and (1 0 4) became narrower and stronger, which was associated with the growth of grains. According to the Scherer formula [22], the particle sizes of the MN powder at 550 °C, 650 °C, 750 °C and 850 °C were calculated to be 36, 42, 42 and 45 nm, respectively. The morphological changes in the as-formed raw nanopowders were illustrated in Fig. 3(a–d). As observed in these images, the particle morphology was substantially altered with the calcination temperatures. It was worth noting that the particles were usually agglomerated due to the high surface to volume ratio and basically regular in shape, just with a substantial variation in particle size at different calcination temperatures. The particle sizes were measured by the liner intercept method [23] and the range of particle sizes was about 30–40, 40–50, 50–60 and 60–70 nm for the samples calcined at 550 °C, 650 °C, 750 °C and 850 °C, respectively. These results indicated that the average particle sizes and agglomeration phenomenon tended to increase with calcination temperatures. Due to the existence of the agglomeration phenomena, the range of particle size was not in good coincidence with the calculated results of Scherer formula. The comparison of MN particle sizes synthesized by different methods was listed in Table 1 and the results showed that the MN powders had smaller particle size of 30–40 nm obtained by the aqueous sol–gel process with larger surface area and free energy, compared with other results as shown in Table 1. Since the surface free energy is considered to be a driving force in the sintering process, a number of sintering models have been researched for the initial stage of sintering and the resulting equation has been deduced. According to the sintering equation of initial stage [24], the use of MN nanopowders as the starting materials was effective in preparing high density MN ceramics through low-temperature sintering and short sintering time. Therefore, the sol–gel process showed significant advantages of sintering the ceramics at relatively low temperatures, which were demonstrated by other reports elsewhere [14–17].

3.2. Characterization and microwave properties of $Mg_4Nb_2O_9$ ceramics

The XRD patterns of MN ceramics sintered at 1150–1325 °C were shown in Fig. 4. The major phases were identified as the ordered corundum structure $Mg_4Nb_2O_9$ with the space group of $P\bar{3}c1$ and still minor secondary phases of $Mg_5Nb_4O_{15}$ with orthorhombic symmetry were observed. The X-ray diffraction patterns of

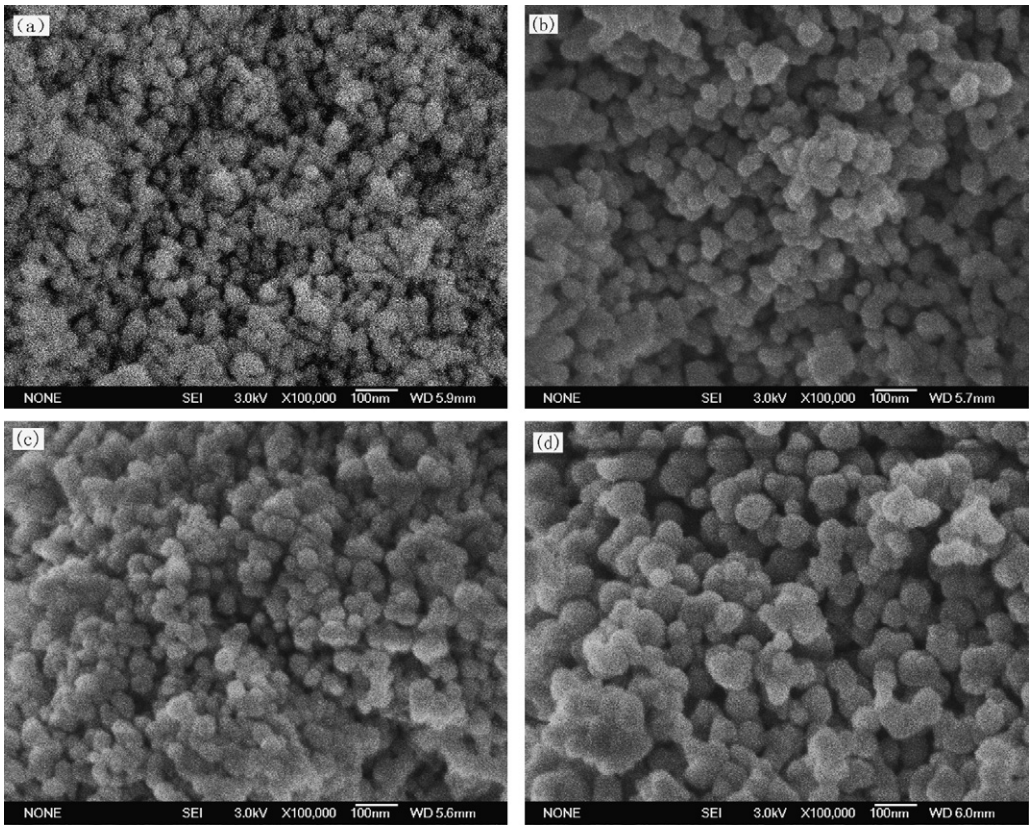

Fig. 3. FE-SEM micrographs of the raw MN nanopowders calcined at (a) 550 °C, (b) 650 °C, (c) 750 °C, and (d) 850 °C for 30 min.

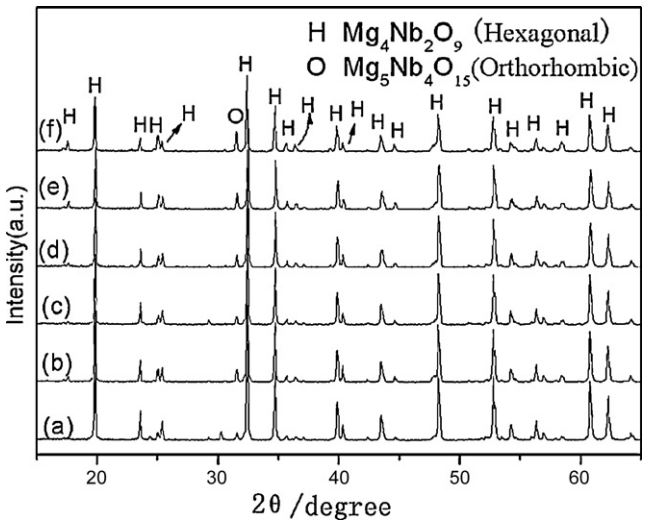

Fig. 4. XRD patterns of MN ceramics sintered at different sintering temperatures ((a–f) corresponding to 1150 °C, 1200 °C, 1250 °C, 1275 °C, 1300 °C, 1325 °C).

the $Mg_4Nb_2O_9$ ceramics system did not have significant change throughout the sintering temperatures range between 1150 and 1325 °C. The SEM images of $Mg_4Nb_2O_9$ ceramics sintered at different temperatures for 4 h were illustrated in Fig. 5. Changes in the porosity and grain size could be seen with an increase in the sintering temperature. The apparent porosity decreased as the sintering temperature increased and all pores disappeared at 1250 °C on the surface of $Mg_4Nb_2O_9$ samples. As the sintering temperature increased, the grain size increased rapidly and the grain size measured by a linear intercept method [23] was about ~3 μm at 1250 °C shown in Fig. 5(c). However, inhomogeneous grain growth was observed above 1250 °C on Fig. 5(d–f) indicated by the arrows, which might be caused by the second growth of grains. Moreover, the grain morphology of $Mg_4Nb_2O_9$ ceramics exhibited two types of grains: large grains and small cubic-shape grains dispersed on the surface of large grains. The concentrations of Mg and Nb ions in the large grains were analyzed to be 34.27 and 20.01 at.%, respectively. The ratio of Mg/Nb was approximately corresponding to the $Mg_4Nb_2O_9$ phase. On the contrast, the concentrations of Mg and Nb ions in the small grains were analyzed to be 43.81 and 32.22 at.%, respectively. The ratio of Mg/Nb was approximately corresponding to the $Mg_5Nb_4O_{15}$ phase. These results were consistent with the above XRD analysis.

Table 2
Microwave dielectric properties of MN ceramics sintered at various temperatures for 4 h in air.

Sintering temperature (°C)	ρ (g/cm^3)	f_0 (GHz)	ε_r	Qf (GHz)	τ_f (ppm/°C)
1150	3.40	10.91	5.7	22,365	−37.8
1200	3.82	10.47	8.6	35,742	−43.6
1250	4.06	9.71	12.3	165,000	−47.5
1275	4.09	9.68	12.3	160,780	−41.3
1300	4.09	9.70	12.4	153,920	−46.9
1325	4.10	9.78	12.6	155,450	−48.7

The apparent densities, dielectric constants, Qf values and τ_f values of the samples dependence on the sintering temperatures were summarized in Table 2. Fig. 6 represented the apparent densities and diametric shrinkage ratio of MN ceramics as a function of sintering temperature, through which the optimized sintering temperature was determined. The apparent densities increased from 3.4 to 4.1 g/cm^3 as the sintering temperature increased from 1150 °C to 1325 °C. A saturated value of apparent densities was obtained at 1250 °C. The curves of the diametric shrinkage ratio showed the similar tendency and also increased with increasing temperature, then saturated at about 1250 °C. It was demonstrated that the MN ceramics were successfully prepared with high density through the sol–gel process at 1250 °C and the sintering temperature was reduced significantly compared to the solid-state reaction method [5,6].

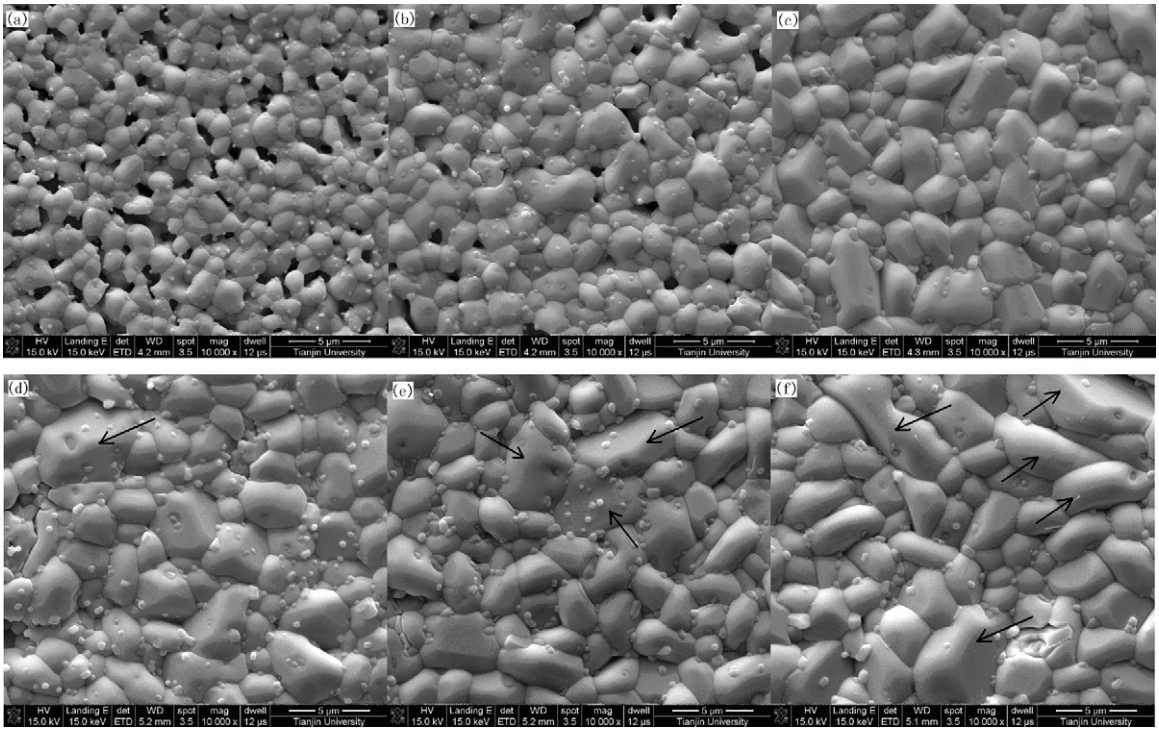

Fig. 5. FE-SEM micrographs of MN ceramics sintered at different sintering temperatures for 4 h ((a–f) corresponding to 1150 °C, 1200 °C, 1250 °C, 1275 °C, 1300 °C, 1325 °C).

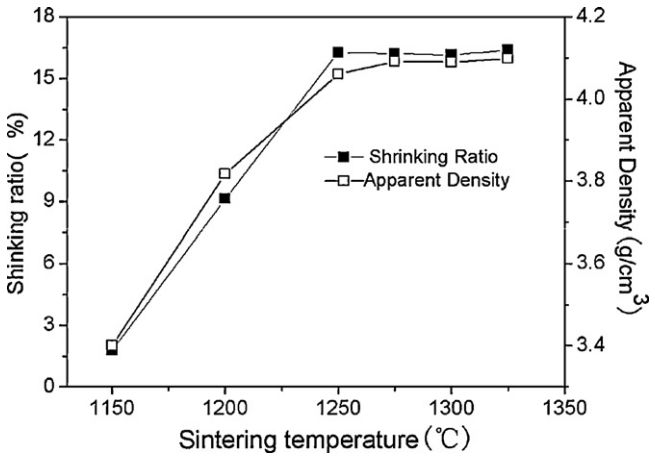

Fig. 6. Relative densities and shrinkaging ratio of MN ceramics as a function of sintering temperatures.

The plots of ε_r, *Qf* and τ_f values were shown in Fig. 7 as a function of sintering temperatures. The ε_r values of MN ceramics steadily increased from 5.7 to 12.6 as the sintering temperature ranged from 1150 °C to 1325 °C. Based on the SEM results, it was obvious that the low ε_r values were caused by the microstructure of MN ceramics with much pores at sintering temperature <1250 °C. The ε_r values were approximately saturated about 12 at sintering temperatures >1250 °C. The curves of ε_r values showed the similar tendency with those of the apparent density and shrinkage ratio, which were sensitive to the dense degree of the microstructure significantly. In general, higher density could achieve higher dielectric constant owing to a lower amount of pores with $\varepsilon_r \sim 1$. In addition, the effect on the dielectric constants caused by the second phase of $Mg_5Nb_4O_{15}$ could be negligible due to its minor quantity and approximate dielectric constant of $\varepsilon_r \sim 11$ reported by Jawahar et al. [25] and Kamba et al. [26]. The results of ε_r values obtained at 1250 °C by the sol–gel process were comparable with these sintered at 1400 °C by the solid-state reaction method [5,6].

With increasing sintering temperatures from 1150 °C to 1325 °C, the *Qf* values increased from 22,365 GHz to 165,000 GHz. The saturated *Qf* values were more than 160,000 GHz at 1250–1275 °C and then a slight decrease appeared at sintering temperatures >1275 °C. The remarkable increase in the *Qf* values ranging from 1150 °C to 1250 °C was related to the reduction of porosity according to the SEM results. Relative density was one of the important factors in controlling the dielectric loss, which had been shown on other microwave dielectric materials. Due to the increased density and appropriate grain growth the $Mg_4Nb_2O_9$ ceramics sintered at 1250 °C had the excellent *Qf* value of 165,000 GHz. Usually, the *Qf* value was independent of the density or porosity for the theoretical density >90% [27]. Therefore, when the sintering temperature was more than 1250 °C, a slight decrease in the *Qf* values was attributed to the significant abnormal grain growth shown on the results of SEM images.

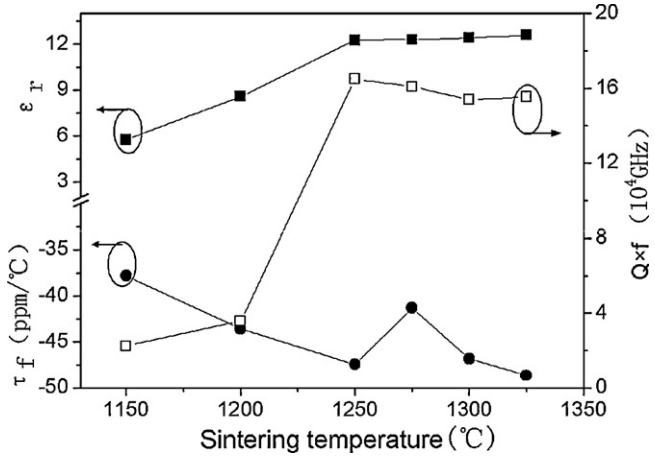

Fig. 7. ε_r, *Qf* and τ_f vs. the sintering temperatures for MN ceramics sintered at 1150 °C, 1200 °C, 1250 °C, 1275 °C, 1300 °C, 1325 °C, respectively.

The *Qf* values of MN ceramics sintered at temperatures from 1150 °C to 1325 °C were significantly high in comparison with those of MN ceramics prepared by the hydrothermal and precipitation methods mentioned above [9,12]. Compared with the results by the solid-state reaction method, Khalam et al. [6] reported a lower *Qf* result of 116,000 GHz, Fu et al. [8] reported a similar *Qf* value of 175,000 by the high-energy ball-milling method, while Kan et al. [5] reported a relatively higher *Qf* value of 193,000. As for the *Qf* values of the dielectric ceramics, it is known that porosity, secondary phase, structure defect and grain boundary of the ceramics produce a deterioration in the *Qf* values [28]. Among these factors, associated with our results the second phase was suggested to affect the *Qf* values obviously. Based on the above XRD results, the formation of $Mg_5Nb_4O_{15}$ phase was detected on the samples sintered at all temperatures shown in Fig. 4. As for the $Mg_5Nb_4O_{15}$ phase, the crystal structure of which was deeply investigated to be isostructural with pseudobrookite of Fe_2TiO_5 by Pagola et al. [29] and Nobuhiro et al. [30], Jawahar et al. [25] and Kamba et al. [26] reported the microwave properties of $Mg_5Nb_4O_{15}$ phase with a *Qf* value of ~37,400 GHz sintered at 1475 °C. According to the well-known general empirical model for multiphase ceramics [31], the presence of the $Mg_5Nb_4O_{15}$ phase inevitably had a significantly detrimental effect on the *Qf* values due to its poor microwave properties. In addition, the $Mg_5Nb_4O_{15}$ phase showed a high sintering temperature of 1475 °C, which was not beneficial to reduce the sintering temperatures. Fortunately, there was a minor amount of $Mg_5Nb_4O_{15}$ phase, which had negligibly detrimental effect on the densification of ceramics. In the next step, it was urgent for us to synthesize the pure MN ceramics through the sol–gel process to eliminate the influence of $Mg_5Nb_4O_{15}$ phase by adjusting the stoichiometric ratio of Mg/Nb in order to improve the microwave properties.

Moreover, the remarkable variations in the τ_f values were not recognized with sintering temperatures from 1150 °C to 1325 °C and these values ranged from −48.7 to −37.8 ppm/°C. Similarly, the minor $Mg_5Nb_4O_{15}$ phase had not significant effect on the τ_f values of MN ceramics due to the approximate τ_f value of −54 ppm/°C. Thus, it was considered that the additional improvement in the τ_f value was required for the dielectric resonator applications at high frequency.

4. Conclusions

The aqueous sol–gel synthetic route was efficiently used to prepare a corundum-structure $Mg_4Nb_2O_9$ phase with the particle sizes below 100 nm, which showed major advantage over the other methods reported before. A considerable decrease in the calcinations temperature (at 550 °C) was obtained in pure oxygen atmosphere for the formation of $Mg_4Nb_2O_9$ nanopowders. Moreover, the sintering ability and microwave properties of $Mg_4Nb_2O_9$ ceramics were systematically investigated at different sintering temperatures. The $Mg_4Nb_2O_9$ samples with nearly full densities were obtained at 1250 °C and showed excellent properties: $\varepsilon_r = 12.3$, *Qf* = 165,000 GHz and $\tau_f = -47.5$ ppm/°C. The results showed that the sol–gel process achieved nanosized powders with larger surface area and high free energy, which was beneficial to reduce the sintering temperature and optimize the performance $Mg_4Nb_2O_9$ ceramics.

References

[1] N.M. Alford, S.J. Penn, J. Appl. Phys. 80 (1996) 5895–5898.
[2] S. Ananta, Mater. Lett. 58 (2004) 2530–2536.
[3] S. Ananta, Mater. Lett. 58 (2004) 2834–2841.
[4] K. Sreedhar, N.R. Pavaskar, Mater. Lett. 53 (2002) 452–455.
[5] H. Ogawa, A. Kan, S. Ishihara, Y. Higashida, J. Eur. Ceram. Soc. 23 (2003) 2485–2488.
[6] L.A. Khalam, S. Thomas, M.T. Sebastian, Int. J. Appl. Ceram. Technol. 4 (2007) 359–366.
[7] R. Wongmaneerung, T. Sarakonsri, R. Yimnirun, S. Ananta, Mater. Sci. Eng. B: Solid 130 (2006) 246–253.
[8] Z.F. Fu, P. Liu, X.M. Chen, J.L. Ma, H.W. Zhang, J. Alloys Compd. 493 (2010) 441–444.
[9] A. Kan, H. Ogawa, J. Alloys Compd. 364 (2004) 247–249.
[10] P.A. Joy, Mater. Lett. 32 (1997) 347–349.
[11] V.V. Deshpande, M.M. Patil, V. Ravi, Mater. Lett. 32 (2006) 353–355.
[12] S.-W. Lim, J. Bang, J. Electroceram. 23 (2009) 116–120.
[13] A.V. Murugan, A.B. Gaikwad, V. Ravi, Bull. Mater. Sci. 29 (2006) 7–9.
[14] S.P. Wu, J.H. Luo, S.X. Cao, J. Alloys Compd. 502 (2010) 147–152.
[15] Q.L. Zhang, F. Wu, H. Yang, J.F. Li, J. Alloys Compd. 508 (2010) 610–615.
[16] Y.C. Zhang, B.J. Fu, Y.H. Liu, X. Wang, T. Li, Z.X. Yue, J. Alloys Compd. 505 (2010) 750–753.
[17] S.A. Hassanzadeh-Tabrizi, E. Taheri-Nassaj, J. Alloys Compd. 494 (2010) 284–289.
[18] K. Guo, H.H. Chen, X.X. Guo, X.X. Yang, F.F. Xu, J.T. Zhao, J. Alloys Compd. 500 (2010) 34–38.
[19] C. Jinga, D. Berger, C. Matei, S. Jinga, E. Andronescu, J. Alloys Compd. 497 (2010) 239–243.
[20] B.W. Hakki, P.D. Coleman, IEEE Trans. 8 (1960) 116–120.
[21] W.E. Courtney, IEEE Trans. 18 (1970) 476–485.
[22] Y.K. Lakshmi, P.V. Reddy, J. Alloys Compd. 470 (2009) 67–74.
[23] A. Thorvaldsen, Acta Mater. 45 (1997) 595–600.
[24] S.-J.L. Kang, Sintering: Densification, Grain Growth & Microstructure, Elsevier Butterworth-Heinemann, Burlington, 2005.
[25] I.N. Jawahar, P. Mohanan, M.T. Sebastian, Mater. Lett. 57 (2003) 4043–4048.
[26] S. Kamba, J. Petzelt, E. Buixaderas, D. Haubrich, P. Vaněk, P. Kužel, I.N. Jawahar, M.T. Sebastian, P. Mohanan, J. Appl. Phys. 89 (2001) 3900–3906.
[27] W.S. Kim, T.H. Hong, E.S. Kim, K.H. Yoon, J. Appl. Phys. 37 (1998) 5367–5371.
[28] S.J. Penn, M.N. Alford, A. Templeton, X. Wang, M. Xu, M. Reece, K. Schrapel, J. Am. Ceram. Soc. 80 (1997) 1885–1888.
[29] S. Pagola, R.E. Carbonio, J.A. Alonso, J. Solid State Chem. 137 (1998) 359–364.
[30] K. Nobuhiro, Y. Yoshinori, T. Takahiro, K. Nobukazu, J. Ceram. Soc. Jpn. 117 (2009) 489–493.
[31] W.D. Kingery, Introduction to Ceramics, 2nd ed., Wiley, New York, 1976.